Inorg. Chem. **2004**, *43*, 8318–8329

High Covalence in $CuSO_4$ and the Radicalization of Sulfate: An X-ray Absorption and Density Functional Study

Robert K. Szilagyi,[†] Patrick Frank,[‡,§] Serena DeBeer George,[§] Britt Hedman,[§] and Keith O. Hodgson*[,‡,§]

Department of Chemistry and Biochemistry, Montana State University, Bozeman, Montana 59717, Department of Chemistry, Stanford University, Stanford, California 94305, and Stanford Synchrotron Radiation Laboratory, SLAC, Stanford University, Stanford, California 94309

Received November 4, 2003

Sulfur K-edge X-ray absorption spectroscopy (XAS) of anhydrous $CuSO_4$ reveals a well-resolved preedge transition feature at 2478.8 eV that has no counterpart in the XAS spectra of anhydrous $ZnSO_4$ or copper sulfate pentahydrate. Similar but weaker preedge features occur in the sulfur K-edge XAS spectra of [Cu(itao)SO_4] (2478.4 eV) and [Cu{$(CH_3)_6$tren}SO_4] (2477.7 eV). Preedge features in the XAS spectra of transition metal ligands are generally attributed to covalent delocalization of a metal d-orbital hole into a ligand-based orbital. Copper L-edge XAS of $CuSO_4$ revealed that 56% of the Cu(II) 3d hole is delocalized onto the sulfate ligand. Hybrid density functional calculations on the two most realistic models of the covalent delocalization pathways in $CuSO_4$ indicate about 50% electron delocalization onto the sulfate oxygen-based 2p orbitals; however, at most 14% of that can be found on sulfate sulfur. Both experimental and computational results indicated that the high covalence of anhydrous $CuSO_4$ has made sulfate more like the radical monoanion, inducing an extensive mixing and redistribution of sulfur 3p-based unoccupied orbitals to lower energy in comparison to sulfate in $ZnSO_4$. It is this redistribution, rather than a direct covalent interaction between Cu(II) and sulfur, that is the origin of the observed sulfur XAS preedge feature. From pseudo-Voigt fits to the $CuSO_4$ sulfur K-edge XAS spectrum, a ground-state 3p character of 6% was quantified for the orbital contributing to the preedge transition, in reasonable agreement with the DFT calculation. Similar XAS fits indicated 2% sulfur 3p character for the preedge transition orbitals in [Cu(itao)SO_4] and [Cu{$(CH_3)_6$tren}SO_4]. The covalent radicalization of ligands similar to sulfate, with consequent energy redistribution of the virtual orbitals, represents a new mechanism for the induction of ligand preedge XAS features. The high covalence of the Cu sites in $CuSO_4$ was found to be similar to that of Cu sites in oxidized cupredoxins, including its anistropic nature, and can serve as the simplest inorganic examples of intramolecular electron-transfer processes.

Introduction

Sulfur K-edge X-ray absorption spectroscopy (XAS) involves sulfur 1s → *n*p electric dipole allowed transitions, i.e., a transition from the sulfur 1s core to an unoccupied sulfur-based orbital with p-type contributions.[1−5] These XAS spectra are sensitive to the sulfur oxidation state, chemical environment, and group symmetry.[6−11] In transition metal oxide,[12−20] chloride,[21−24] and thiolate[3−5,25,26] complexes, a ligand XAS preedge feature arises from a covalent ligand−metal interaction that mixes filled ligand 2p or 3p valence orbitals with the unoccupied metal 3d orbitals. This interaction produces partially unoccupied molecular orbitals with

* To whom correspondence should be addressed: Prof. Keith O. Hodgson. Tel.: 1-650-926-3153. Fax: 1-650-926-4100. E-mail: Hodgson@ssrl.slac.stanford.edu.
† Montana State University.
‡ Department of Chemistry, Stanford University.
§ Stanford Synchrotron Radiation Laboratory, SLAC, Stanford University.

(1) Hedman, B.; Frank, P.; Gheller, S. F.; Newton, W. E.; Solomon, E. I.; Hodgson, K. O. *Physica B* **1989**, *158*, 71−73.
(2) Tyson, T. A.; Roe, A. L.; Frank, P.; Hodgson, K. O.; Hedman, B. *Phys. Rev. B* **1989**, *39*, 6305−6315.
(3) Shadle, S. E.; Penner-Hahn, J. E.; Shugar, H. J.; Hedman, B.; Hodgson, K. O.; Solomon, E. I. *J. Am. Chem. Soc.* **1993**, *115*, 767−776.
(4) Rose, K.; Shadle, S. E.; Eidsness, M. K.; Kurtz, D. M., Jr.; Scott, R. A.; Hedman, B.; Hodgson, K. O.; Solomon, E. I. *J. Am. Chem. Soc.* **1998**, *120*, 10743−10747.
(5) Glaser, T.; Hedman, B.; Hodgson, K. O.; Solomon, E. I. *Acc. Chem. Res.* **2000**, *33*, 859−868.
(6) Hedman, B.; Frank, P.; Penner-Hahn, J. E.; Roe, A. L.; Hodgson, K. O.; Carlson, R. M. K.; Brown, G.; Cerino, J.; Hettel, R.; Troxel, T.; Winick, H.; Yang, J. *Nucl. Instr. Methods* **1986**, *A246*, 797−800.

10.1021/ic030311l CCC: $27.50
Published on Web 12/03/2004

significant ligand 2p or 3p character.[12,27,28] These orbitals are generally at lower energy than the unoccupied ligand 3p or 4p virtual orbitals that are responsible for the rising absorption edge features in ligand K-edge XAS spectra.[3,5] Thus, a ligand-based preedge transition derived from the partially unoccupied metal−ligand molecular orbital appears at lower energy than the nominal ligand XAS rising K-edge.[4,5,26,29,30]

While investigating the sulfur K-edge XAS spectra of monodentate sulfate compounds, we noted an unexpected transition feature in the energy region just below the main rising-edge energy in the XAS spectra of [Cu(II){$(CH_3)_6$-tren}SO_4] and [Cu(itao)SO_4]. These trigonal-bipyramidal complexes (Figure 1) include an axial sulfate ligand.[31,32] As noted above, the appearance of a preedge transition in the K-edge XAS spectrum of sulfate can imply the presence of a new unoccupied bound state lower in energy than the sulfur 4p-based ($6t_2$, see below) virtual orbital of the sulfate anion[33−35] responsible for the intense features of the XAS rising-edge absorption.

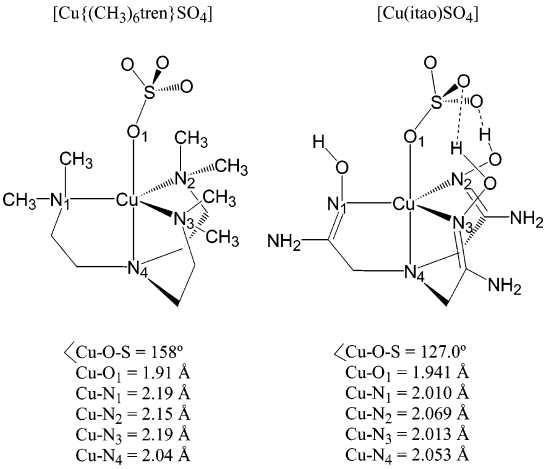

Figure 1. Relevant structural metrics of [Cu{$(CH_3)_6$tren}SO_4][31] and [Cu(itao)SO_4].[32]

To investigate this phenomenon, we measured the sulfur K-edge XAS spectra of anhydrous $CuSO_4$ and found an intense preedge feature at lower energy than the sulfate rising-edge energy. Here, we report the results of a systematic study of the sulfur K-edge XAS spectra of anhydrous $CuSO_4$, anhydrous $ZnSO_4$, copper sulfate pentahydrate, and the two Cu(II)-OSO_3 trigonal-bipyramidal complexes noted above. The sulfur K-edge XAS spectra and the L-edge (2p → *n*d) XAS spectrum[36,37] of anhydrous $CuSO_4$ are reported, followed by the results of density functional theory (DFT) calculations elucidating the covalent delocalization pathways within the $CuSO_4$ lattice. These pathway models are herein used to provide a theoretical understanding of how the electronic structure of the sulfate ion is modified by the direct Cu(II)−sulfate electronic interactions. Finally, pseudo-Voigt fits to the sulfur K-edge XAS spectra of all of these compounds were used to refer the covalence of anhydrous $CuSO_4$ back to covalence in the monodentate Cu(II)−sulfate complexes.

Materials and Methods

Sample Preparation. [Cu(itao)SO_4] was prepared by the method of Pearse et al.,[32] including synthesis of the ligand (imino-tris-acetamidoxime). [Cu{$(CH_3)_6$tren}SO_4] was prepared by the method of Anderegg and Gramlich.[31] The ligand, tris(*N*,*N*-dimethyl-2-aminoethyl)amine, [$(CH_3)_6$tren], was prepared by the method of Ciampolini and Nardi.[38] Anhydrous >99.99% $CuSO_4$ was purchased from Aldrich Chemicals and used as received. Anhydrous $ZnSO_4$ was prepared by dehydrating the heptahydrate (Baker Analyzed) overnight at 280 °C.[39,40] Loss upon drying of the

(7) Sekiyama, H.; Kosugi, N.; Kuroda, H.; Ohta, T. *Bull. Chem. Soc. Jpn.* **1986**, *59*, 575−579.
(8) Frank, P.; Hedman, B.; Carlson, R. M. K.; Tyson, T. A.; Roe, A. L.; Hodgson, K. O. *Biochemistry* **1987**, *26*, 4975−4979.
(9) George, G. N.; Gorbaty, M. L. *J. Am. Chem. Soc.* **1989**, *111*, 3182−3186.
(10) Frank, P.; Hedman, B.; Carlson, R. M. K.; Hodgson, K. O. *Inorg. Chem.* **1994**, *33*, 3794−3803.
(11) Frank, P.; Hedman, B.; Hodgson, K. O. *Inorg. Chem.* **1999**, *38*, 260−270.
(12) Grunes, L. A. *Phys. Rev. B* **1983**, *27*, 2111−2131.
(13) Troeger, L.; Arvanitis, D.; Rabus, H.; Wenzel, L.; Baberschke, K. *Phys. Rev. B* **1990**, *41*, 7297−7300.
(14) Kurata, H.; Colliex, C. *Phys. Rev. B* **1993**, *48*, 2102−2108.
(15) Ma, Y.; Johnson, P. D.; Wassdahl, N.; Guo, J.; Skytt, P.; Nordgren, J.; Kevan, S. D.; Rubensson, J. E.; Boeske, T.; Eberhardt, W. *Phys. Rev. B* **1993**, *48*, 2109−2111.
(16) SchedelNiedrig, T.; Weiss, W.; Schlogl, R. *Phys. Rev. B* **1995**, *52*, 17449−17460.
(17) Soldatov, A. V.; Povahzynaja, N. A.; Shvejtzer, I. G. *Solid State Commun.* **1996**, *97*, 53−58.
(18) Wu, Z. Y.; Gota, S.; Jollet, F.; Pollak, M.; Gautier-Soyer, M.; Natoli, C. R. *Phys. Rev. B* **1997**, *55*, 2570−2577.
(19) Uchimoto, Y.; Sawada, H.; Yao, T. *J. Synchrotron Radiat.* **2001**, *8*, 872−873.
(20) Näslund, L.-A.; Cavalleri, M.; Ogasawara, H.; Nilsson, A.; Pettersson, L. G. M.; Wernet, P.; Edwards, D. C.; Sandström, M.; Myneni, S. *J. Phys. Chem. A* **2003**, *107*, 6869−6876.
(21) Hedman, B.; Hodgson, K. O.; Solomon, E. I. *J. Am. Chem. Soc.* **1990**, *112*, 1643−1645.
(22) Shadle, S. E.; Hedman, B.; Hodgson, K. O.; Solomon, E. I. *Inorg. Chem.* **1994**, *33*, 4235−4244.
(23) Shadle, S. E.; Hedman, B.; Hodgson, K. O.; Solomon, E. I. *J. Am. Chem. Soc.* **1995**, *117*, 2259−2272.
(24) Rompel, A.; Andrews, J. C.; Cinco, R. M.; Wemple, M. W.; Christou, G.; Law, N. A.; Pecoraro, V. L.; Sauer, K.; Yachandra, V. K.; Klein, M. P. *J. Am. Chem. Soc.* **1997**, *119*, 4465−4470.
(25) Atanasov, M.; Potze, R. H.; Sawatzky, G. A. *J. Solid State Chem.* **1995**, *119*, 380−393.
(26) Williams, K. R.; Hedman, B.; Hodgson, K. O.; Solomon, E. I. *Inorg. Chim. Acta* **1997**, *263*, 315−321.
(27) Neese, F.; Hedman, B.; Hodgson, K. O.; Solomon, E. I. *Inorg. Chem.* **1998**, *38*, 4854−4860.
(28) Szilagyi, R. K.; Lim, B. S.; Glaser, T.; Holm, R. H.; Hedman, B.; Hodgson, K. O.; Solomon, E. I. *J. Am. Chem. Soc.* **2003**, *125*, 9158−9169.
(29) Williams, K. R.; Gamelin, D. R.; LaCroix, L. B.; Houser, R. P.; Tolman, W. B.; Mulder, T. C.; de Vries, S.; Hedman, B.; Hodgson, K. O.; Solomon, E. I. *J. Am. Chem. Soc.* **1997**, *119*, 613−614.
(30) Glaser, T.; Rose, K.; Shadle, S. E.; Hedman, B.; Hodgson, K. O.; Solomon, E. I. *J. Am. Chem. Soc.* **2001**, *123*, 442−454.
(31) Anderegg, G.; Gramlich, V. *Helv. Chim. Acta* **1994**, *77*, 685−690.
(32) Pearse, G. A.; Raithby, P. R.; Maughan, M. M. *Polyhedron* **1994**, *13*, 553−558.
(33) Adachi, H.; Taniguchi, K. *J. Phys. Soc. Jpn.* **1980**, *49*, 1944−1953.
(34) Connor, J. A.; Hillier, I. H.; Wood, M. H.; Barber, M. *J. Chem. Soc., Faraday Trans. 2* **1974**, *8*, 1040−1044.
(35) Johansen, H. *Theor. Chim. Acta (Berlin)* **1974**, *32*, 273−278.
(36) George, S. J.; Lowery, M. D.; Solomon, E. I.; Cramer, S. P. *J. Am. Chem. Soc.* **1993**, *115*, 2968−2969.
(37) DeBeer George, S.; Metz, M.; Szilagyi, R. K.; Wang, H.; Cramer, S. P.; Lu, Y.; Tolman, W. B.; Hedman, B.; Hodgson, K. O.; Solomon, E. I. *J. Am. Chem. Soc.* **2001**, *123*, 5757−5767.
(38) Ciampolini, M.; Nardi, N. *Inorg. Chem.* **1966**, *5*, 41−44.
(39) Berg, L. G.; Pribylov, K. P. *Khim. Khim. Tekhnol.* **1964**, *7*, 535−539; *Chem. Abstr.* **1965**, *62*, 13800.

anhydrous $ZnSO_4$ at 300 °C (Galbraith Labs) was <0.36%, indicating <0.032 of a residual water molecule per $ZnSO_4$ unit. The anhydrous sulfates were stored and were prepared for XAS measurement within an inert-atmosphere glovebox (Vacuum Atmospheres). Reagent-grade cupric sulfate pentahydrate (Aldrich Chemicals) was recrystallized by slow evaporation of a saturated solution.

Sulfur K-edge XAS Measurements. Sulfur K-edge spectra were measured on SSRL beamline 6-2 under dedicated operating conditions of 3 GeV and 50−100 mA, with a wiggler field of 1.04 T. The X-ray beam was energy-resolved using a Si[111] double-crystal monochromator, which was fully tuned at 2740 eV. Harmonic contamination was removed using a Ni-coated rejection mirror. The data were calibrated against the first absorption maximum of sodium thiosulfate, which was set at 2472.02 eV. Thiosulfate calibration spectra were measured before and after every three data scans. The XAS data were processed as has been described in detail previously.[10,11] The sulfur K-edge spectra were fit with pseudo-Voigt lines over the energy range 2476−2486 eV using the program EDG_FIT.[41] Pseudo-Voigt lines consist of a 1:1 sum of Gaussian and Lorentzian line shapes. A minimum number of pseudo-Voigt lines were used while requiring that the half-widths at half-maximum (HWHM) be 0.5 ± 0.1 eV, in keeping with spectrometer resolution and sulfur core−hole lifetime broadening.[42] During the fits, the HWHM of the pseudo-Voigt peaks were linked and co-refined over the range 2480−2486 eV. The fits were considered acceptable if they reproduced both the XAS spectrum and the second derivative of the XAS spectrum.[43] Multiple fits that produced slightly different background intensities in the preedge energy region indicated an error range of ±6% in the total integrated area of the pseudo-Voigts used to fit to the preedge features of the spectra. All solid samples were finely ground in boron nitride and spread in a thin translucent layer on sulfur-free Mylar tape to minimize self-absorption artifacts. The X-ray 1/e attenuation depth for pure $CuSO_4$ is about 1.8 μm,[44] which is similar to that of pure sulfur.[45]

Cu L-edge XAS Measurements. Cu L-edge spectra were measured using the SSRL 31-pole wiggler beam line 10-1, using a wiggler field of 1.45 T. Samples were finely ground and spread across double-adhesive conductive carbon tape (SPI Supplies, West Chester, PA), which was attached to an aluminum sample holder. The data were measured at room temperature as total electron yield spectra utilizing a Galileo 4716 channeltron electron multiplier as a detector. Three scans were measured to check reproducibility. The energy was calibrated from the Cu L-edge spectra of CuF_2, run at intervals between sample scans. The maxima of the L_3 and L_2 preedges of CuF_2 were assigned to 930.5 and 950.5 eV, respectively. Data were processed as described previously.[37] A linear background was fit to the L_3 preedge region (870−920 eV) and was subtracted from the entire spectrum. The spectra were normalized by fitting a straight line to the postedge region and scaling the edge jump to 1.0 at 1000 eV. Fits to the edges were performed using the program EDG_FIT.[41] Pseudo-Voigt peaks were used to model the L_3 and L_2 2p → 3d transitions. Arctangent functions were used to model the L_3 and L_2 edge jumps. The total L preedge intensity reported here was calculated as the sum of the L_3 and L_2 intensities. The reported intensity value is based on the average of all good fits. Normalization procedures can introduce ~4% error in preedge peak intensities, in addition to the error resulting from the fitting procedure.

Density Functional Calculations. Gradient-corrected, hybrid density functional calculations were carried out using the Gaussian 98 package[46] on a 32 CPU SGI Origin2000 supercomputer. The Becke88 exchange[47] and Perdew86[48] correlation nonlocal functionals were used with Vosko−Wilk−Nusair local functionals[49] as implemented in the software package (BP86). The triple-ζ-quality, Gaussian-type all-electron basis set was employed with polarization function for the Cu (6-311G*) and a double-ζ basis set with polarization for the oxygen and sulfur atoms (6-31G*). Because the standard GGA type calculations (BP86) overestimate the covalence of ligand−metal bonding in Cu(II)-containing complexes, 38% HF exchange was mixed into the total exchange functional. The B(38HF)P86 method has been extensively tested on various Cu(II)-containing complexes[50] and bioinorganic active site models[51] and found to give reasonable ground- and excited-state bonding descriptions. In addition, various population analysis methods were evaluated and showed that the spin densities vary at most 7%.[51] The atomic coordinates of the computational models shown in Figure 2 were taken from the X-ray structure of anhydrous $CuSO_4$ (Figure 3)[52,53] and are provided as Supporting Information. The $S = 3$, 2, and 1 states were selected for the ground states of the six-, four-, and two-Cu models with total charges of $Z = +10$, $+6$, and $+2$, respectively, because $CuSO_4$ is paramagnetic at room temperature,[54,55] at which the sulfur K-edge data were measured. Spherically arranged neutralizing point charges at about 3 Å distance from the outermost atoms affected only the absolute values of the orbital energies and had insignificant influence on the orbital splitting and coefficients.

(40) Spiess, M.; Gruehn, R. *Z. Anorg. Allg. Chem.* **1979**, *456*, 222−240; *Chem. Abstr.* **1980**, *92*, 103563.
(41) This program is available free of charge as part of the EXAFSPAK software package at http://www-ssrl.slac.stanford.edu/exafspak.html.
(42) Krause, M. O.; Oliver, H. H. *J. Phys. Chem. Ref. Data* **1979**, *8*, 329−338.
(43) Frank, P.; Hodgson, K. O. *Inorg. Biochem* **2000**, *39*, 6018−6027.
(44) The algorithm to calculate this value is available at the Web site of the Lawrence Berkeley Laboratory: http://www-cxro.lbl.gov/optical_constants/.
(45) Pickering, I. J.; George, G. N.; Yu, E. Y.; Brune, D. C.; Tuschak, C.; Overmann, J.; Beatty, J. T.; Prince, R. C. *Biochemistry* **2001**, *27*, 8138−8145.
(46) Frisch, M. J.; Trucks, G. W.; Schlegel, H. B.; Scuseria, G. E.; Robb, M. A.; Cheeseman, J. R.; Montgomery, J. A., Jr.; Vreven, T.; Kudin, K. N.; Burant, J. C.; Millam, J. M.; Iyengar, S. S.; Tomasi, J.; Barone, V.; Mennucci, B.; Cossi, M.; Scalmani, G.; Rega, N.; Petersson, G. A.; Nakatsuji, H.; Hada, M.; Ehara, M.; Toyota, K.; Fukuda, R.; Hasegawa, J.; Ishida, M.; Nakajima, T.; Honda, Y.; Kitao, O.; Nakai, H.; Klene, M.; Li, X.; Knox, J. E.; Hratchian, H. P.; Cross, J. B.; Adamo, C.; Jaramillo, J.; Gomperts, R.; Stratmann, R. E.; Yazyev, O.; Austin, A. J.; Cammi, R.; Pomelli, C.; Ochterski, J. W.; Ayala, P. Y.; Morokuma, K.; Voth, G. A.; Salvador, P.; Dannenberg, J. J.; Zakrzewski, V. G.; Dapprich, S.; Daniels, A. D.; Strain, M. C.; Farkas, O.; Malick, D. K.; Rabuck, A. D.; Raghavachari, K.; Foresman, J. B.; Ortiz, J. V.; Cui, Q.; Baboul, A. G.; Clifford, S.; Cioslowski, J.; Stefanov, B. B.; Liu, G.; Liashenko, A.; Piskorz, P.; Komaromi, I.; Martin, R. L.; Fox, D. J.; Keith, T.; Al-Laham, M. A.; Peng, C. Y.; Nanayakkara, A.; Challacombe, M.; Gill, P. M. W.; Johnson, B.; Chen, W.; Wong, M. W.; Gonzalez, C.; Pople, J. A. *Gaussian 98*, revision A.11; Gaussian, Inc.: Pittsburgh, PA, 1998.
(47) Becke, A. D. *Phys. Rev. A: Gen. Phys.* **1988**, 3098−3100.
(48) Perdew, J. P. *Phys. Rev. B: Condens. Matter Mater Phys.* **1986**, *33*, 8822−8824.
(49) Vosko, S. H.; Wilk, L.; Nusair, M. *Can. J. Phys.* **1980**, *58*, 1200−1211.
(50) Szilagyi, R. K.; Metz, M.; Solomon, E. I. *J. Phys. Chem. A* **2002**, *106*, 2994−3007.
(51) Solomon, E. I.; Szilagyi, R. K.; DeBeer George, S.; Bausmallick, L. *Chem. Rev.* **2004**, *104*, 419−458.
(52) Kokkoros, P. A.; Rentzeperis, P. J. *Acta Crystallogr.* **1958**, *11*, 361−364.
(53) Wildner, M.; Giester, G. *Mineral. Petrol.* **1988**, *39*, 201−209.
(54) Stout, J. W. *J. Chem. Phys.* **1941**, *9*, 285.
(55) Wells, J. S.; Matarrese, L. M.; Sukle, D. J. *J. Chem. Phys.* **1967**, *47*, 2259−2262.

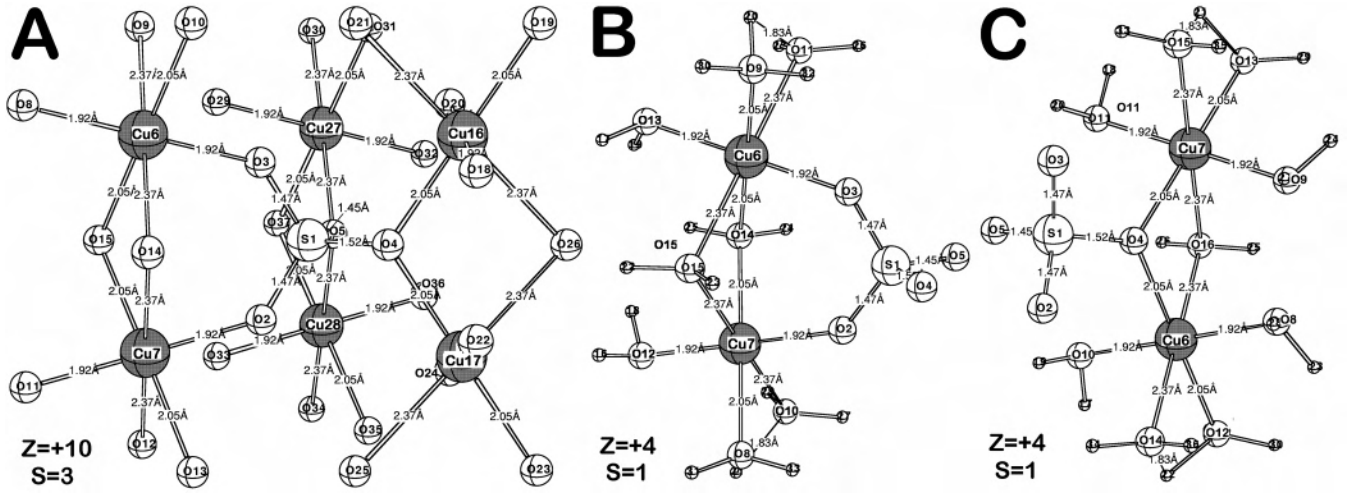

Figure 2. Computational models of anhydrous $CuSO_4$: (A) complete 5.1 Å environment of a sulfate anion (hydrogen atoms on terminal and bridging ligands omitted for clarity); most reasonable models for Cu−sulfate covalent delocalization pathways with (B) three- and (C) two-atom-bridged two-Cu models.

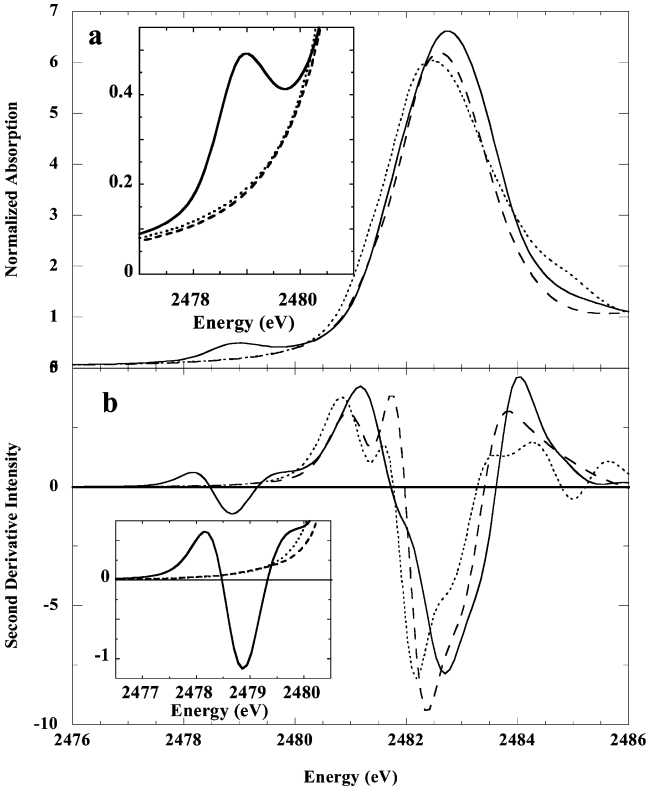

Figure 3. (a) Sulfur K-edge XAS spectra and (b) second derivatives of the XAS spectra of (—) anhydrous $CuSO_4$, (− − −) copper sulfate pentahydrate, and (···) anhydrous $ZnSO_4$ all measured as solids finely ground in BN. Insets are expansions of the preedge energy region showing the unique $CuSO_4$ XAS feature at 2478.8 eV.

It should be noted that the discussed orbital energy levels from DFT calculations correspond to a ground-state description. An absorption feature requires the creation of a hole in the sulfur 1s orbital; hence, an increase of sulfur Z_{eff} and a consequent energy stabilization of sulfur-based occupied orbitals (i.e., final-state relaxation effects) can be expected that are proportional to the amount of sulfur character in the excited state. These excited-state features are more pronounced for rising-edge features, as they involve bound states high in energy relative to core → LUMO excitations.

Results

Sulfate XAS Preedge Features. Figure 3 compares the sulfur K-edge spectra of anhydrous $CuSO_4$, copper sulfate pentahydrate, and anhydrous $ZnSO_4$. In a typical sulfate K-edge XAS spectrum, the main absorption feature near 2482 eV derives from the intense transition of the sulfur 1s electron to the triply degenerate unoccupied $6t_2$ (sulfur 4p-based, Figure S1) orbital.[33,35,56] The second derivatives of the XAS spectra in Figure 3B show that the transitions in the energy range of 2481.5 and 2483.5 eV are split because of the decreased symmetry of sulfate. In copper sulfate pentahydrate, covalent bonding is restricted to the four equatorial waters. The axial interactions between Cu(II) and sulfate ions are Jahn−Teller elongated and primarily electrostatic.[57] The crystal structures of anhydrous $CuSO_4$ and $ZnSO_4$ are isomorphous (Figure 4).[52,53] However, $CuSO_4$ is electronically distinguished from $ZnSO_4$ by a singly occupied 3d orbital that permits covalent metal−ligand orbital mixing and ligand character delocalization.

The sulfur K-edge XAS spectrum of anhydrous $CuSO_4$ in Figure 3 (solid line) shows a preedge feature at 2478.8 eV that is relatively intense compared to the normalized K-edge spectrum of unoxidized sulfur.[45] This unique feature is missing from the K-edge XAS spectra of both $ZnSO_4$ and copper sulfate pentahydrate and reflects the distinctive covalence in the equatorial interaction between sulfate and the unoccupied 3d orbital of Cu(II). Further differences carry through to the main absorption envelope, most clearly evident in Figure 3B, where the shapes of the XAS spectra of $ZnSO_4$ and copper sulfate pentahydrate are comparatively similar over the 2481−2484 eV range, but are quite different from that of anhydrous $CuSO_4$. In addition, the absorption maxima of $ZnSO_4$ and copper sulfate pentahydrate are at lower energy than that of anhydrous $CuSO_4$. These observations indicate that the metal−sulfate bond in anhydrous $CuSO_4$ modified the higher-lying sulfate virtual orbitals. The spectra of both

(56) Sugiura, C. *Jpn. J. Appl. Phys.* **1993**, *32*, 3509−3514.
(57) Varghese, J. N.; Maslen, E. N. *Acta Crystallogr.* **1985**, *B41*, 184−190.

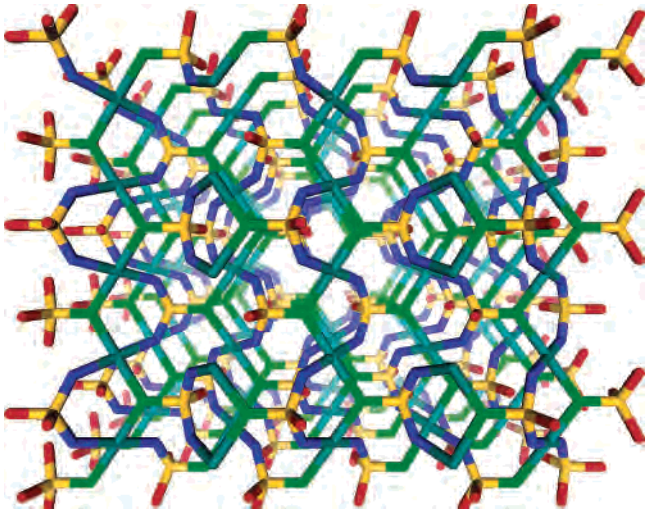

Figure 4. Experimental structure[52,53] of the anhydrous $CuSO_4$ (yellow, sulfur; turquoise, copper; red, green, and blue, oxygens along Cu−O 2.37-, 2.05-, and 1.92-Å vectors, respectively).

$ZnSO_4$ and copper sulfate pentahydrate also exhibit a transition under the rising edge at 2481.4 eV (Figure 3B) that jointly distinguishes them from anhydrous $CuSO_4$. However, the 2.6 eV energy difference makes these features unlikely to correspond to a transition to the same virtual orbital as that producing the preedge feature at 2478.8 eV. Within anhydrous $ZnSO_4$, the interaction of sulfate with the metal ion is primarily electrostatic through six direct Zn−sulfate interactions[52] in addition to involvement of Zn 4s/4p orbitals. No preedge feature has been reported in the XAS spectra of solid Na_2SO_4 or is observed in the XAS spectrum of sulfate in solution.[7,10,11,56,58]

Figure 5 shows the preedge features found in the sulfur K-edge XAS spectra of the monodentate Cu(II)−sulfate complexes [Cu{$(CH_3)_6$tren}SO_4] and [Cu(itao)SO_4] at 2477.7 and 2478.4 eV, respectively. Although each complex is trigonal-bipyramidal overall, the respective Cu−O−S angles (Figure 1) are very different in part because of the presence of two internal hydrogen bonds in the latter complex. The equatorial N atoms in the [Cu{$(CH_3)_6$tren}SO_4] complex are also better donors than those in the [Cu(itao)SO_4] complex. The energy positions of the two preedge transitions are 1.1 and 0.4 eV lower in energy than the analogous feature in the XAS spectrum of anhydrous $CuSO_4$ and are much less intense (Figure 5, Tables S1−S3). These differences should originate from a Cu(II)−sulfate interaction. The coexistence of a preedge sulfate feature in the sulfur K-edge XAS spectra of all complexes with an open-shell Cu(II)−sulfate interaction, along with an absence of this feature in the XAS of the complexes lacking such an interaction, implies a bonding unique to open d-shell transition metals.

Copper Covalence From L-edge XAS. To further investigate the Cu(II)−sulfate covalent interaction in anhydrous $CuSO_4$, the copper L-edge (2p → 3d) XAS spectrum was measured. Transition metal L-edge XAS spectra can be used to measure metal−ligand covalence and indicate the

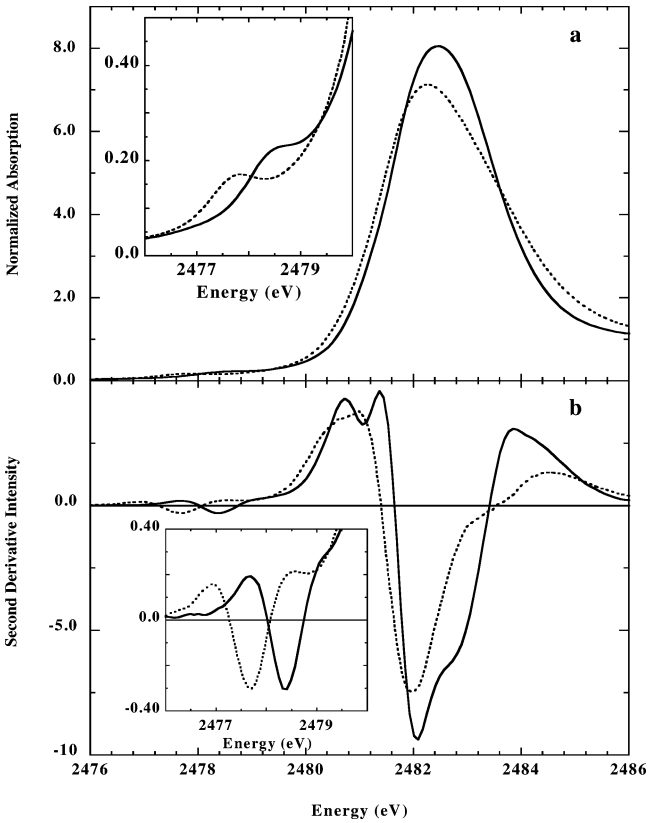

Figure 5. (a) Sulfur K-edge XAS spectra and (b) second derivatives of the XAS spectra of (—) solid [Cu(itao)SO_4] and (···) solid [Cu{$(CH_3)_6$tren}SO_4]. Insets are expansion of the preedge energy region showing the presence of features at 2478.4 and 2477.7 eV, respectively.

extent of electron donation from the ligand into the metal 3d acceptor orbitals.[36,37] Initial reference was made to the percent copper character in the HOMO of (D_{4h}) $[CuCl_4]^{2-}$, which is based on exclusively experimental results such as g values and metal hyperfine and ligand superhyperfine coupling constants obtained from EPR spectroscopy, as well as from analysis of absorption and photoelectron spectroscopy.[59,60] These spectral methods give an average experimental value of 61 ± 2% 3d character in the HOMO of (D_{4h}) $[CuCl_4]^{2-}$. Figure 6 shows a comparison of the Cu L_3-edge spectra for $CuSO_4$ and tetragonal (D_{4h}) $[CuCl_4]^{2-}$. Using $[CuCl_4]^{2-}$ as a reference, for which 8.52 integrated normalized intensity units corresponds to 61% Cu character,[36] the integrated area for $CuSO_4$ (6.15 units) corresponds to 44% 3d character in the singly occupied HOMO. This shows a dramatic electron donation from the sulfate to the Cu and indicates that there is a large covalent interaction in the HOMO of $CuSO_4$. It is also relevant to note that the Cu L-edge is ∼0.8 eV lower in energy than that of D_{4h} $[CuCl_4]^{2-}$. This likely reflects the significant decrease in the relative effective nuclear charge of the copper atom in $CuSO_4$, as well as changes in the ligand field splitting of the d-manifold. These changes in the electronic structure of the copper ion are consistent with Cu(II) becoming more

(58) Xia, K.; Weesner, F.; Bleam, W. F.; Bloom, P. R.; Skyllberg, U. L.; Helmke, P. A. *Soil Sci. Soc. Am. J.* **1998**, *62*, 1240−1246.

(59) Didziulis, S. V.; Cohen, S. L.; Gewirth, A. A.; Solomon, E. I. *J. Am. Chem. Soc.* **1988**, *110*, 250−268.

(60) Gewirth, A. A.; Cohen, S. L.; Schugar, H. J.; Solomon, E. I. *Inorg. Chem.* **1987**, *26*, 1133−1146.

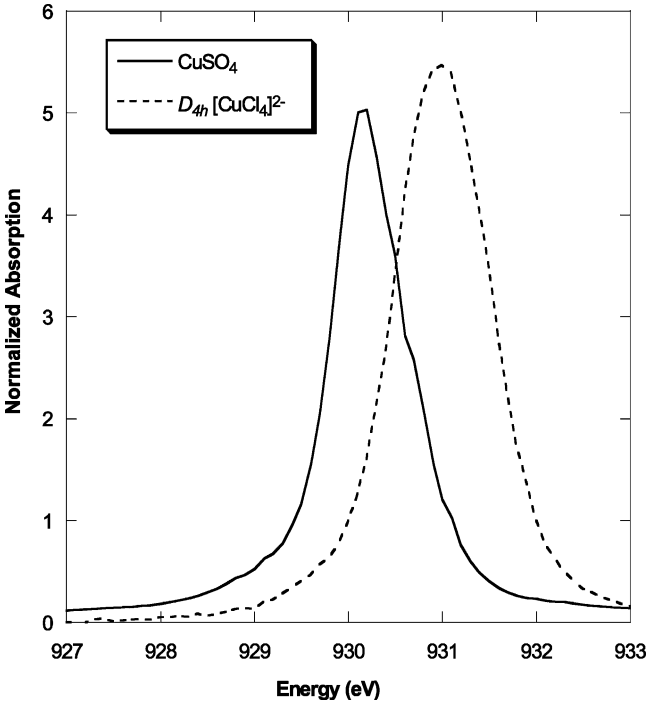

Figure 6. Comparison of the normalized Cu L_3-edge spectra for anhydrous $CuSO_4$ and D_{4h} $[CuCl_4]^{2-}$.

Cu(I)-like. The Cu spin density from L-edge XAS is used below to test and validate the computational models for the covalent delocalization pathways in the $CuSO_4$ lattice.

DFT Calculations of Sulfate Orbitals. To explore the changes in the electronic structure of the transition metal bound sulfate, a systematic density functional study was carried out starting with the sulfate dianion (T_d symmetry with average crystallographic S−O distances of 1.48 Å from the crystal structure of $CuSO_4$),[61] followed by an increase in the complexity of the computational model up to reasonable models for the metal−sulfate interactions in anhydrous $CuSO_4$ and $ZnSO_4$. These calculations employed the spectroscopically calibrated B(38HF)P86 hybrid GGA-type functional with saturated basis set as described in the Materials and Methods section.

The eight occupied and virtual frontier orbitals of sulfate with orbital energies relative to the LUMO are shown in Figure 7A (orbital plots are shown in Figure S1). The energetically most favorable, triply degenerate HOMO ($1t_1$) and HOMO − 1 ($5t_2$) orbitals for donor interaction with transition metals show very little sulfur character (at most 2% f-character in the HOMO and 8% d- and 5% p-character in the HOMO − 1 orbitals). The near absence of sulfur character in the $1t_1$ and $5t_2$ orbitals does not support the assignment of the 2478.8 eV sulfate XAS preedge feature of $CuSO_4$ to covalent delocalization of the Cu(II) valence hole into sulfate HOMO/HOMO − 1 orbitals. In addition, the occurrence of these orbitals at about 8 eV below the sulfur 3p/4p-based rising-edge features places them too low in energy to match the energy position of the observed sulfur preedge XAS feature in $CuSO_4$.

(61) Nord, A. G. *Acta Chem. Scand.* **1973**, *27*, 814−822.

In contrast to the occupied orbitals, the virtual orbitals of sulfate are mainly sulfur-based. The LUMO ($6a_1$) consists of a sulfur 4s orbital with antibonding oxygen 2p interactions along the S−O bonds, as does the $7a_1$ orbital. The LUMO + 1 ($6t_2$) is a triply degenerate set of orbitals derived from the three sulfur 4p orbitals with small oxygen 2p contributions. The next three degenerate orbitals ($7t_2$) correspond to the sulfur 3p and oxygen 2p antibonding orbitals of the S−O bonds with significant sulfur 3d character. The $6a_1$ and $7t_2$ orbitals can be considered as the antibonding orbitals of the S−O bonds.

The symmetry of the sulfate anion in anhydrous $CuSO_4$ is reduced to C_s because of interactions with the surrounding Cu(II) ions and other sulfate anions in the crystal lattice. The reduced symmetry introduces significant orbital splitting and mixing (compare Figure 7A to 7B). The degeneracy of the t-symmetry orbitals is removed, and they split into in-plane (a′) and out-of-plane (a″) orbitals. However, the overall sulfur character of the highest occupied orbitals does not change, and the sulfur p character is no more than 4% in lower-lying occupied orbitals such as 16a′, 6a″, and 15a′. However, the unoccupied orbitals show an interesting redistribution of sulfur character. Because of the T_d to C_s distortion, the sulfate dianion LUMO gains significant sulfur p character through mixing of the $6a_1$ and $6t_2$ orbitals. In the sulfur K-edge spectrum, this would correspond to intensity redistribution of the most intense absorption feature (white line) to lower energy in addition to the broadening of all features in C_s relative to T_d. In Figure 3B, the shoulders at 2481.5 and 2481.7 eV on the low-energy side of the white line can be correlated with $6a_1$ orbitals that include sulfur p mixing and the features on the high-energy side with sulfur $1s \rightarrow 7t_2$ transitions.

As the C_s sulfate is embedded in a field of point charges to mimic the electrostatic field around a sulfate unit in the $CuSO_4$ crystal, as modeled by six +2.0 point charges of the Cu ions and twenty −0.6 point charges of the oxygen atoms from the neighboring sulfate ions, the virtual orbitals further split and mix, giving a more dramatic redistribution of unoccupied sulfur p-type orbitals (Figure 7B versus 7C). This mixing represents changes in the O−S bonding interaction as a result of electron density redistribution induced by the external electrostatic field. It is important to note the distance dependence of the point-charge calculations. If the point charge−sulfate distances are increased by 50% to approximately 3 Å, the observed changes between Figure 7B and 7C drops by 70% (estimated from the change in the electron population on sulfur). At about 5 Å, only the absolute energies of the orbitals are affected without any change in the splitting or in their composition. If the ∼4% sulfur 3p character in the oxygen donor orbitals (e.g., 16a′) were responsible for the preedge XAS feature, through mixing with the Cu(II) 3d hole, the 7−8 eV splitting between the 16a′ and the 19a′/9a″/20a′ orbitals would require the preedge feature to be present about 6−7 eV lower in energy than the rising edge. This estimate assumes approximately 1−2 eV orbital relaxation due to the creation of a hole in the sulfur 1s orbital, but is about 4−5 eV greater than the

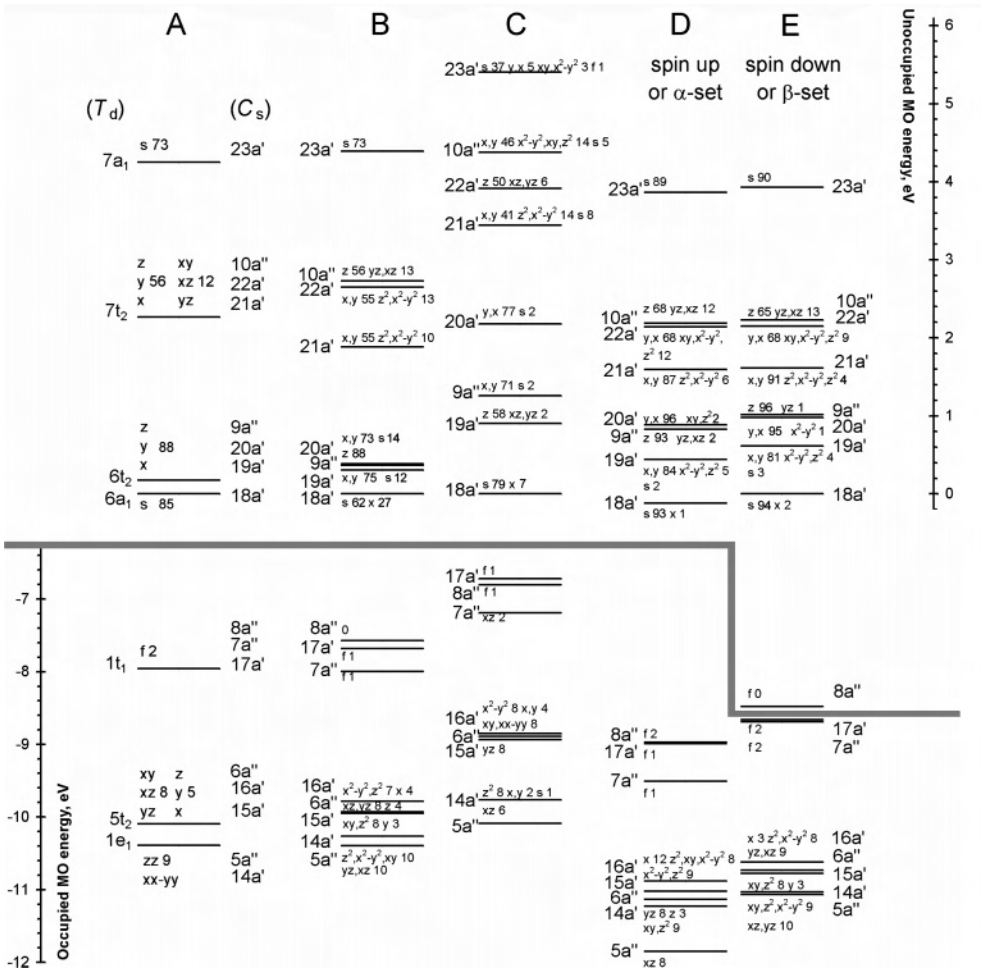

Figure 7. Molecular orbital energy levels and their sulfur contributions in (A) T_d and (B) C_s $[SO_4]^{2-}$ as in the crystal structure of anhydrous $CuSO_4$; (C) C_s $[SO_4]^{2-}$ within the field of +2 and −0.6 charges at the crystallographic positions of neighboring Cu and O atoms, respectively; (D,E) spin-unrestricted α and β orbitals, respectively, of the C_s $[SO_4]^{-}$ radical anion.

observed energy separation between the preedge feature and the first rising-edge inflection of $CuSO_4$ (Figure 3). In addition, anhydrous $CuSO_4$ and $ZnSO_4$ are isostructural, and the $T_d \rightarrow C_s$ distortion and the electrostatic field around sulfate are identical in the two salts. Therefore, if the sulfate XAS preedge feature of $CuSO_4$ stemmed from the electrostatic-induced redistribution of virtual orbitals, the analogous XAS feature would also be visible in the sulfur K-edge spectrum of $ZnSO_4$. In summary, neither electrostatics nor Cu(II) d-hole delocalization into occupied valence levels can be the origin of the sulfur K-edge XAS preedge feature of $CuSO_4$.

DFT Modeling of the Copper-Sulfate Interactions in $CuSO_4$. An appropriate computational model of the $CuSO_4$ lattice should both reproduce the covalence revealed by the copper L-edge XAS spectrum and explain the sulfur K-edge XAS spectrum. Several models were tested, and we describe here only the most relevant ones. The structurally most complete computational model of the $CuSO_4$ lattice included all possible interactions between a C_s sulfate anion and the nearest six Cu(II) ions (Figure 2A). This model is consistent with a 5.1 Å environment of the sulfur atom (excluding the H atoms used to terminate the water ligands in the model). All Cu(II) ions are six-coordinate with two short (1.92 Å), two intermediate (2.05 Å), and two long (2.37 Å) Cu−O vectors as in the crystal structure, and they can be arranged into three well-defined pairs on the basis of their positions relative to the sulfate. Cu6 and Cu7 are expected to give the strongest covalent interaction (three-atom-bridged model) between the Cu(II) and the sulfate ions[62] with the shortest Cu−O (1.92 Å) and S−O (1.47 Å) distances. The sets of atoms O8, O10, O3, and O15 with Cu6 and O11, O13, O2, and O15 with Cu7 (blue-colored O atoms in Figure 4) define the planes of the singly occupied Cu 3d orbitals, which can accept electron density from the sulfate because of efficient overlap. Similarly, the Cu16 and Cu17 bridged by O4 are covalently linked to the sulfate (one-atom-bridged model), providing an additional pathway for covalent interactions (green colored O atoms in Figure 4). Cu27 and Cu28 are different from the four other Cu sites, as they are connected to the sulfate O5 along the axial direction with respect to the singly occupied Cu 3d orbital, and hence, they are involved in only electrostatic interaction with the sulfate. The peripheral sulfate oxygen atoms could be terminated by oxide, hydroxide, water, or hydronium ligands. All of these possibilities were tested, and we discuss the most reasonable

(62) Reynolds, P. A.; Figgis, B. N. *J. Phys. Condens. Matter* **1991**, *3*, 1977−1983.

Table 1. Cu−SO_4 Atomic Spin Densities for the Non-hydrogen Atoms in the Computational Models Shown in Figure 2 Calculated at the B(38HF)P86/BS5 Level of Theory by Mulliken Population Analysis

six-Cu model (Figure 2A)[a]		two-Cu model, 1.92 Å (Figure 2B)		two-Cu model, 2.05 Å (Figure 2C)	
atom	spin	atom	spin	atom	spin
S1	0.011	S1	−0.133	S1	−0.196
O2	0.024	O2	0.075	O2	0.370
O3	0.026	O3	0.075	O3	0.370
O4	0.046	O4	0.755	O4	0.095
O5	0.007	O5	0.328	O5	0.483
Cu6	0.792	Cu6	0.395	Cu6	0.393
Cu7	0.797	Cu7	0.395	Cu7	0.393
Cu16	0.795	O8[c]	0.013	O8[b]	0.030
Cu17	0.800	O9[c]	0.013	O9[b]	0.030
Cu27	0.793	O10[d]	0.002	O10[b]	0.039
Cu28	0.800	O11[d]	0.002	O11[b]	0.039
		O12[b]	0.029	O12[c]	0.019
		O13[b]	0.029	O13[c]	0.019
		O14[c]	0.065	O14[d]	0.003
		O15[d]	0.008	O15[d]	0.003
				O16[d]	0.006

[a] O_w atoms are omitted for clarity. [b−d] Cu−O distances are 1.92, 2.05, and 2.37 Å for superscripts *b*−*d*, respectively.

models below. The oxide and hydroxide ligands were not useful, because they are significantly better donors than the sulfate and they reduce the copper−sulfate interaction to a few percent, which is inconsistent with the copper L-edge XAS result. The trigonal prismoidal arrangement of Cu(II) ions and peripheral sulfate oxygen atoms modeled as terminal and bridging water molecules in the six-Cu model produced an isotropic ligand environment around the sulfate anion and did not allow for significant electron density donation from the sulfate to the Cu (Table 1). In particular, the covalent metal−ligand interactions in the six-Cu model are dominated by the peripheral water molecules, rendering this model physically inappropriate for the description of covalent interactions between the Cu(II) and sulfate ions. In a truncated six-Cu model without any of the water ligands, the orientation of the Cu 3d orbitals is not restricted by the local ligand field symmetry, and only limited electron density (0.04 e) is donated from the sulfate to each of the Cu ions. The isotropic environment is still maintained in a four-Cu model without Cu27 and Cu28 and the water ligands. These limitations of the electronic structures did not allow for the use of an extended computational model for $CuSO_4$ lattice, because none of them reproduced the Cu L-edge results.

Instead of attempting to establish a nonperiodic structural model for the $CuSO_4$ lattice, we constructed computational models that can describe the intramolecular electron transfer between the sulfate and Cu(II). The most reasonable models for the Cu−sulfate covalent interactions are shown in Figure 2B and 2C, which contain the two pathways for the covalent Cu−sulfate interactions found in the extended lattice. Taken together, they should allow for a reasonable explanation of the covalent bonding within anhydrous $CuSO_4$ and help to define the origin of the preedge feature in the S K-edge XAS. To model the anisotropy in the ligand field environment around the Cu(II) ions and produce agreement between the calculated and experimental Cu 3d character of the ground-state wave function, two water ligands in each model were protonated (O8 and O9 in Figure 2B and O12 and O13 in Figure 2C), giving a hydrogen-bonding interaction (H···O distances are 1.83 Å) with the other equatorial water ligands (O10 and O11 in Figure 2B and O14 and O15 in Figure 2C) while maintaining the overall C_s symmetry of the models. This hydrogen-bonding interaction weakens the donor strength of the peripheral water ligands and rotates the Cu $3d_{x^2-y^2}$ orbital to give good overlap with the sulfate donor orbitals. It is worth noting that the atomic spin densities were affected by less than 5% upon variation of the location of the two protons on the equatorial water ligands. A bridging protonation of the terminal waters can also be justified in terms of the nominal bond order of the sulfate oxygen atoms in $CuSO_4$, which is 3.5 for O4, O5 and 2.5 for O2, O3 compared to 1.5 in isolated sulfate. Partial protonation lowers the electron-donating ability of the terminal waters to be more commensurate with that of the bridging sulfate oxygen atoms, creating an anisotropic environment around the sulfate that is more similar to the covalent bonding channels within the extended lattice of $CuSO_4$. It is important to emphasize that parts B and C of Figure 2 are models for the Cu−sulfate interaction and not for the sulfate environment. In addition, without the protonation, the Cu spin densities would be too high by at least 30% relative to the Cu L-edge data. The atomic spin densities calculated for the two-Cu models are summarized in Table 1. The wave functions of the two models are similar, but different $1t_1$-type sulfate orbitals (Figure S1) are involved in bonding. Figure S2 shows the atomic spin density plots for the two models and illustrates this difference graphically. On the other hand, in both models, the Cu spin density is around 0.40 electron, which has 93% Cu 3d character and is within a very reasonable 4% agreement with the Cu L-edge XAS results (44%, see above). The water ligands donate only about 0.20 electron, while the rest originates from the sulfate. The sulfur atoms have negative spin densities with 10% s-, 70% p-, and 20% d-character, which is indicative of spin polarization due to a greater mixing of β (spin-down) virtual and occupied orbitals relative to the α (spin-up) orbitals. In the anhydrous $CuSO_4$ crystal, the two Cu−sulfate covalent interactions exist simultaneously and involve two energetically degenerate but spatially different sulfate donor orbitals, allowing for an efficient (at most 56% per sulfate) electron delocalization.

Overall, spectroscopically calibrated DFT studies suggest two well-defined intramolecular electron delocalization pathways between the sulfate anion and the neighboring Cu(II) ions. These are the three-atom-bridged Cu−O−S−O−Cu path with the shortest Cu−O distances of 1.92 Å and the one-atom-bridged Cu−O−Cu path with Cu−O distances of 2.05 Å. The two interactions are about equally important in defining pathways for the Cu−Cu superexchange interactions. The covalent interactions in the anhydrous $CuSO_4$ crystal uniquely affect the mixing and the energy levels of the sulfate virtual orbitals, which can produce a bound state with nonnegligible sulfur p-character lower in energy than the nominal $6t_2$ unoccupied MOs of an isolated sulfate anion.

$[SO_4]^-$ within $CuSO_4$. The ground-state wave function of the anhydrous $CuSO_4$ based on Cu L-edge results corresponds to an electronic structure in which the copper ions are closer to a d^{10} Cu(I) ionic limit, and from DFT calculations the unpaired electrons, or the corresponding electron holes, are localized on primarily oxygen-based sulfate orbitals. This state of the sulfate can be reasonably approximated by a monoanionic $[SO_4]^-$ radical. Figure 6D and 6E shows the α and β orbital energy levels of the spin-unrestricted, open-shell wave function for the sulfate radical in the experimental C_s geometry.

The splitting of the corresponding orbitals in the mono- and dianionic sulfates are quite different. This difference in splitting can be correlated with the different sulfur K-edge rising-edge features of the $CuSO_4$ and $ZnSO_4$ samples. The βLUMO of the $[SO_4]^-$ radical (the first orbital above the gray line in Figure 6E), which is only slightly separated from the βHOMO, has no sulfur orbital character and clearly cannot contribute any intensity to a transition in a sulfur K-edge XAS spectrum. Rather, the preedge feature in $CuSO_4$ arises from the unique intensity redistribution of rising-edge features that derive from sulfur-based unoccupied orbitals (mixing of virtual orbitals is summarized in Figure S3). This redistribution toward lower energy has its origin in the strong covalent interaction between the singly occupied Cu(II) 3d orbital and the occupied frontier oxygen 2p-based orbitals of the sulfate dianion. Covalence delocalizes the electron density from the sulfate onto copper, changing the purely diamagnetic electronic structure of sulfate as found within anhydrous $ZnSO_4$, while conversely the copper becomes more like the d^{10} Zn(II) ion.

In $ZnSO_4$, the 3d orbital is completely filled, and the covalent 3d-orbital-based valence-level interaction is absent. The preedge feature is therefore also absent, and bonding in $ZnSO_4$ is dominated by electrostatic interactions with a limited diamagnetic Zn(II) 4s/4p orbital-based interaction. The electronic structure of the sulfate in $ZnSO_4$ is consistent with the orbital energy levels of the sulfate dianion as shown in Figure 7B.

Orbital Assignment of the Sulfate XAS Preedge Features. Figure 8 shows the sulfur 3p and 4p distributions of the virtual orbitals calculated for the two-Cu pathway models (Figure 2B and 2C). Ligand preedge XAS features based on donor orbitals normally originate from sulfur 1s to LUMO transitions, and LUMO + n in the case of multiple (n + 1) electron holes. However, from Figure 8, the sulfur p character of these orbitals is zero. The next 7 eV energy range above the LUMO also does not show any significant sulfur p character, because these virtual orbitals are based on various mixtures of Cu 4s/4p and water orbitals with a small contribution of sulfate oxygen 2p orbitals. In the $CuSO_4$ crystal, these orbitals would contain only metal 4s/4p and sulfate O contributions. However, the αLUMO + 19, βLUMO + 17 and the αLUMO + 18, βLUMO + 17 in the three- and one-atom-bridged, two-Cu pathway models, respectively, include 56−64% Cu 4s, 7−5% sulfur 3p, and 4−3% sulfate O character. These two orbitals occur about 1−2 eV below the onset of the main rising edge, which can

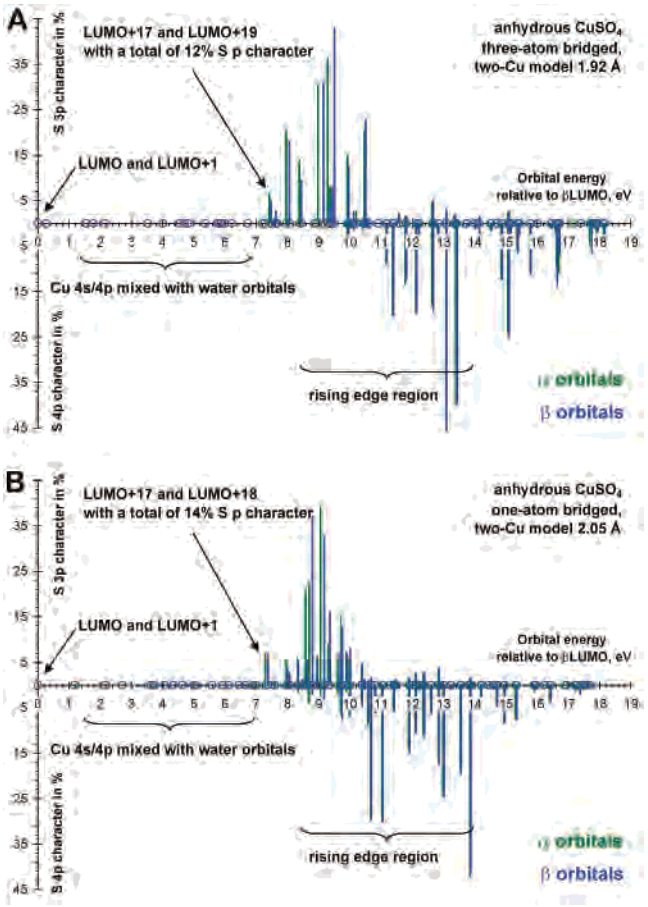

Figure 8. Distribution of sulfur 3p and 4p character of the unoccupied orbitals for the computational model complex in the two-Cu models.

be estimated from the energy position of unoccupied orbitals with greater sulfur 3p/4p characters. These suggest the possibility of mixing Cu 4s and sulfate unoccupied orbitals with sulfur 3p contribution ($7t_2$), giving the most reasonable origin of the preedge feature in the sulfur K-edge spectrum of anhydrous $CuSO_4$. Orbitals at higher energy give rise to the intense rising-edge features, and about 17 eV above the LUMO, the sulfur p-orbital contribution diminishes. This high-energy region corresponds to various unbound states, where the photoelectron has enough energy to enter the continuum. Similarly, low-energy, unoccupied orbitals can be identified with nonnegligible sulfur 3p character for the two monodentate complexes as shown in Figure S4A and S4B. Figure S4C and S4D shows the lowest unoccupied orbitals for the isostructural $ZnSO_4$ models to those of in Figure 2B and 2C without any significant mixing of Zn 4s/4p and sulfate orbitals in the lowest 9 eV energy range relative to the LUMO. Orbitals above 9 eV already have a large sulfur character and contribute to the rising edge.

Any change in the occupied orbitals affects the unoccupied counterparts as well. Thus, the order of the sulfur 3p- and 4p-based orbitals has changed in the two-Cu pathway models, compared to the uncoordinated anion (see Figures 8 and 7B). In conversion of dianionic C_s sulfate to the monoanionic radical sulfate (Figure 7A versus 6D and 6E), mixing of lower-lying 4p-based (19a′, 20a′, and 9a″) and higher-lying 3p-based (21a′, 22a′, and 10a″) orbitals occurs (see Figure

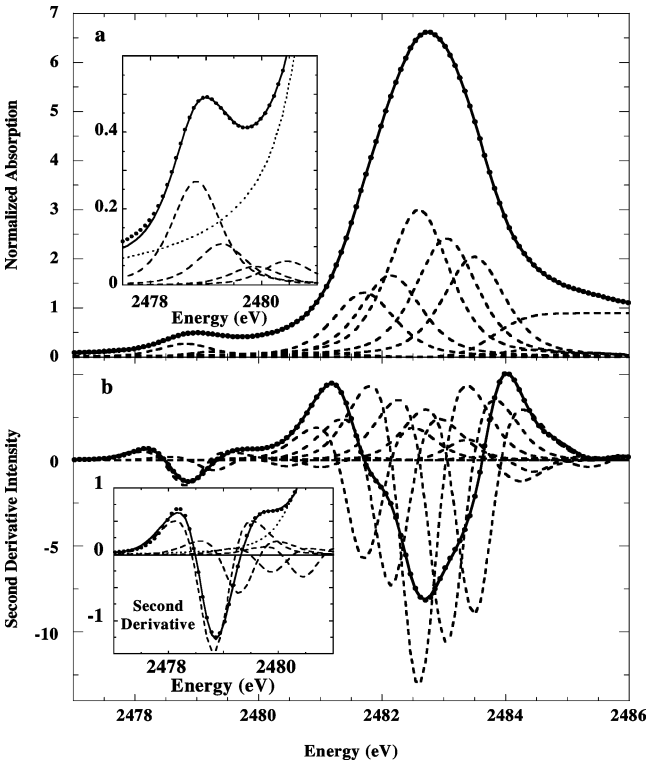

Figure 9. (a) Pseudo-Voigt fit to the sulfur K-edge XAS spectrum and (b) second derivative of the XAS spectrum of anhydrous $CuSO_4$: (●) XAS data, (−) fit to the data, and (− − −) pseudo-Voigt lines. Arctangent representing the ionization threshold appears at 2483.81 eV (− − −). Insets show the fit to the XAS spectra in the preedge energy region.

S3), which redistributes the sulfur 3p and 4p orbital contributions. The result is a complete switch in the energy ordering of these orbitals in the pathway models. This inversion can be rationalized by significant electron donation from the occupied sulfate orbitals to the Cu(II) ions, resulting in weaker S−O bonds. This in turn reduces the splitting of the S−O bonding and antibonding combinations of sulfur 3p and oxygen 2p atomic orbitals. The energy position of the sulfur 4p orbitals does not change significantly, because the electron donation is primarily from the oxygen of the S−O bond (see the highest occupied orbitals in Figure S2).

Sulfur 3p Character in the Sulfate XAS Preedge Features. The XAS spectra in Figure 5 indicate a similar, though much smaller, direct covalent interaction between Cu(II) and sulfate in [Cu{$(CH_3)_6$tren}SO_4] and [Cu(itao)-SO_4]. Sulfur K-edge XAS preedge features attending transition metal sulfates and phosphates have been reported previously; however, the features were assigned to delocalization of the metal 3d hole into a sulfur valence-level orbital.[63]

Figure 9 shows the pseudo-Voigt fit to the sulfur K-edge XAS spectrum of $CuSO_4$. Following the criteria described in the Materials and Methods section, this fit produced a set of features within the main absorption envelope comparable in number and energy separation to the orbital array predicted by the DFT calculation (Figure 7D and 7E). Good fits were also obtained for the sulfur XAS spectra of [Cu(itao)SO_4] and [Cu{$(CH_3)_6$tren}SO_4] under the same criteria (Figures S5 and S6 and Tables S1−S3). These fits were carried out over the entire energy range of the XAS K-edge spectra in order to provide physically valid background intensity for the pseudo-Voigts fit to the preedge features, which were then used to estimate sulfur 3p character (see below).

As noted above, the intensity of the preedge transition correlates with the amount of 3p character in the ground-state orbital of origin. The contribution of 3p orbitals to the intensity of the preedge transitions can be calculated from the transition dipole integral, $I(S)$, and the integrated intensity (i.e., the peak area) of the preedge transition.[3] $I(S)$ is related to the effective nuclear charge, Z_{eff}, of the sulfur absorber and the integrated transition intensity reflects the sulfur 3p character of the probed unoccupied orbital. The transition dipole integral for sulfate in the Cu(II)−SO_4 complexes can be evaluated from the energy position of the second-derivative minima of the sulfur K-edge XAS spectra corresponding to a sulfur 1s → 4p transition by reference to the known values for other sulfur ligands.[28] The results of this calculation for $CuSO_4$, [Cu(itao)SO_4], and [Cu{$(CH_3)_6$tren}-SO_4] are reported in Table 2, with $ZnSO_4$ and solution sulfate as references. For $CuSO_4$, the preedge transition is found to have 6% sulfur 3p character, in reasonable agreement with the polarized neutron diffraction study (3%) and also with the DFT pathway models in Figure 2B and 2C (12% and 14%, respectively), which reproduce the Cu L-edge results within 4%. The covalence of the Cu−OSO_3 bond in the two monodentate complexes was estimated using the relative areas of the preedge features obtained from the pseudo-Voigt fits (Table 2) with the assumption of a linear relationship. These estimates predict that the Cu(II)−OSO_3 bonds in [Cu(itao)SO_4] and [Cu{$(CH_3)_6$tren}SO_4] are equivalently covalent, but are much less covalent than in $CuSO_4$. That is, the radicalization of sulfate is relatively less in the two complexes. Spectroscopically calibrated DFT calculation gives 74% and 78% Cu and 15% and 13% total sulfate spin densities, respectively, for the two monodentate complexes with less than 8−11% sulfur 3p character in orbitals that are reasonable candidates for the preedge features. We intend to test the inherent assumption for the structurally well-defined model complexes in the future by directly determining the copper−sulfate covalence in [Cu(itao)SO_4] and [Cu{$(CH_3)_6$tren}SO_4] through the copper L-edge spectroscopy.

It is noteworthy that the values of $I(S)$ in Table 2 indicate a higher Z_{eff} for sulfate in neutral aqueous solution than sulfate in the two monodentate complexes or in $ZnSO_4$. The second-derivative minimum of the sulfur K-edge spectrum of copper sulfate pentahydrate is coincident with that of solution sulfate. Thus, the relative Z_{eff} values of the sulfur atom in sulfate is $CuSO_4 \gg [SO_4]^{2-}$(aq), $CuSO_4 \cdot 5H_2O > ZnSO_4 >$ [Cu(itao)SO_4], [Cu{$(CH_3)_6$tren}SO_4]. The surprising aspect of this ordering is the positions of solution sulfate and of sulfate in $CuSO_4 \cdot 5H_2O$ relative to sulfate in anhydrous $ZnSO_4$. This trend in Z_{eff} is also evident in Figure 3, which shows that both the rising XAS K-edge and the absorption

(63) Okude, N.; Nagoshi, M.; Noro, H.; Baba, Y.; Yamamoto, H.; Sasaki, T. A. *J. Electron Spectrosc. Relat. Phenom.* **1999**, *101−103*, 607−610.

Table 2. Experimental Covalence in the Cupric−Sulfate Bond

complex	preedge intensity[a]	white-line energy, eV	2nd-deriv minimum, eV	$I(S)$[b]	S 3p (α^2)[c] (%)	% sulfate covalence (%)
$CuSO_4$ (anhydr)	0.430	2482.8	2482.7	20.82	6	56[d]
$[Cu\{(CH_3)_6tren\}SO_4]$	0.107	2482.3	2481.9	19.77	2	14[e]
$[Cu(itao)SO_4]$	0.118	2482.5	2482.1	19.97	2	15[e]
$ZnSO_4$ (anhydr)	−	2482.4	2482.2	20.13	−	−
$[SO_4]^{2-}$ (aq)[f]	−	2482.5	2482.3	20.27	−	−

[a] Total integrated area of the pseudo-Voigt lines fitting the preedge feature, in normalized units; estimated error is ±7%. [b] Transition moment integral evaluated from the linear relation with the XAS energy of the second-derivative minimum corresponding to sulfur 1s → 4p transitions.[28] [c] Sulfur contribution to the orbital represented by the pre-K-edge transition, calculated from the expression integrated intensity = $D_0 = (A/3n)\alpha^2 I(S)$, where A is the ground-state degeneracy (1) and n is the number of sulfur atom absorbers.[28] [d] Determined experimentally as $[1 - \alpha^2(Cu)]$, where $\alpha^2(Cu)$ was measured from the copper L-edge XAS spectrum (see text). [e] Estimated value relative to sulfate in $CuSO_4$. [f] In pH 6.3 aqueous solution.

maximum of sulfate in $ZnSO_4$ occur at lower energy than those of $CuSO_4$ or $CuSO_4 \cdot 5H_2O$. Possibly accounting for this trend, sulfate engages multiple hydrogen bonds in water solution[64−66] as well as in $CuSO_4 \cdot 5H_2O$,[57,67] dispersing the large negative charge more thoroughly than in $ZnSO_4$. Lower electron density in ligand valence orbitals decreases the shielding of the core electrons from the nuclear charge, thus increasing Z_{eff}.

Discussion

The 44% Cu(II) 3d character in the HOMO of anhydrous $CuSO_4$ is comparable in magnitude to the total covalence of the copper sites in the blue copper protein plastocyanin (41%)[36] and the Cu_A site in cytochrome *c* oxidase (44%).[37] These sites feature Cu(II)−S(Cys) bonds, which are noteworthy for their very high covalence. Considerable spin delocalization from the metal 3d orbitals to the ligand is generally regarded as a feature unique to the electron-transfer proteins, and the highly covalent Cu−S(thiolate) bonds are essential to the efficient electron-transfer function of these sites. An analogous covalence is thus not typically observed in inorganic complexes consisting of Cu(II) bonded to second-row main-group atoms. For example, in crystalline $[Cu(H_2O)_6]^{2+}$, the total Cu(II) 3d character is about 75%.[68,69] Even in La_2CuO_4, wherein Cu(II) is surrounded by a distorted octahedron of dianionic oxide ions (4O at 1.90 Å, 2O at 2.40 Å) that exhibits structural metrics comparable to those of the copper site in $CuSO_4$, a Cu(II) 3d character of 62% was found.[70] The equivalent covalence of $CuSO_4$ with blue Cu(II)−thiolate protein sites reflected by the Cu character from Cu L-edge XAS spectra is particularly unexpected given that $E°$ for the reaction $2H^+ + S_2O_8^{2-} + 2e^- \rightleftharpoons 2\,HSO_4^-$ is 2.1 V, whereas the comparable value for cysteine is calculated to be 0.77 V (for the thiol−disulfide interchange).[71,72] The primary difference in the Cu−ligand covalence between the inorganic salt and the bioinorganic active site is in the nature of the ligand donor orbitals. The thiolate donor orbitals are located exclusively on one sulfur atom directly attached to the metal, whereas in sulfate, they are equally delocalized among the four O atoms without significant sulfur character. XAS is thus a powerful experimental technique to detect saddle changes in metal−ligand bonding beyond the atoms directly connected to the metal.

Preedge peaks in the K-edge XAS spectra of ligands bonded directly to unfilled 3d orbitals of transition metals are due to the mixing of occupied p-character ligand orbitals and unoccupied metal 3d orbitals. However, the results described here now show that there can be an additional origin for preedge features in ligand K-edge spectra. This source is the mixing and redistribution of unoccupied ligand virtual orbitals to lower energy induced by a covalent interaction with a metal ion. This interaction corresponds to an internal redox reaction. When sulfate is bonded to transition metals with unfilled d orbitals, intramolecular electron transfer occurs from ligand to metal, originating from an orbital consisting primarily of oxygen 2p-based contributions. This internal electron transfer produces a radical character in the ligand that causes an extensive remixing of virtual orbitals. In sulfate, the unoccupied sulfur 3p−oxygen 2p antibonding orbitals mix with metal 4s, 4p at lower energy and give rise to an XAS preedge feature below the rising-edge jump. The presence of this preedge feature is an indicator of metal−ligand covalence, but it reflects a mechanism that is completely distinct from the situation in which the ligand absorber is directly bonded to the metal. The analogue of the XAS preedge transition seen, for example, in transition metal thiolates or chlorides, for the Cu(II)-OSO_3 bond should occur in the oxygen K-edge[20] of sulfate and *not* at the sulfur K-edge as a result of delocalization of the metal 3d hole into the HOMO of sulfate consisting of the oxygen 2p-based orbitals. Using the Cu L-edge and sulfur K-edge results of $CuSO_4$, an experimental transition dipole can be defined and utilized in O K-edge measurements.

Finally, any preedge transitions in the K-edge XAS spectra of the central element of oxoanionic transition metal ligands, such as sulfate, phosphate,[63] chlorate, arsenate, or selenate, will all most likely derive from the same radicalization mechanism. Therefore, the appearance of a preedge feature in the K-edge XAS spectra of such ligands is diagnostic of

(64) Magini, M. J. *Chem. Phys.* **1979**, *70*, 317−324.
(65) Caminiti, R.; Paschina, G.; Pinna, G.; Magini, M. *Chem. Phys. Lett.* **1979**, *64*, 391−395.
(66) Caminiti, R. *Chem. Phys. Lett.* **1982**, *88*, 103−108.
(67) Bacon, G. E.; Titterton, D. H. *Z. Kristallogr.* **1975**, *141*, 330−341.
(68) Getz, D.; Silver, B. L. *J. Chem. Phys.* **1974**, *61*, 630−637.
(69) Radhakrishna, S.; Rao, T. B. *J. Magn. Reson.* **1978**, *32*, 71−81.
(70) Tranquada, J. M.; Heald, S. M.; Kunnmann, W.; Moodenbaugh, A. R.; Qiu, S. L.; Xu, Y. *Phys. Rev. B* **1991**, *44*, 5176−5188.
(71) Eldjarn, L.; Pihl, A. *J. Am. Chem. Soc.* **1957**, *79*, 4589−4593.
(72) Szajewski, R. P.; Whitesides, G. M. *J. Am. Chem. Soc.* **1980**, *102*, 2011−2026.
(73) Kennepohl, P.; Solomon, E. I. *Inorg. Chem.* **2003**, *42*, 689−695.

a bond to a transition metal with unfilled d orbitals and so should prove useful in deducing bonding interactions in complex materials.

Acknowledgment. This work was supported by Grants NIH RR-01209 (to K.O.H.) and NSF EPSCOR (to R.K.S.). We thank the Center for Computational Biology at MSU for computational time on a Silicon Graphics Origin 2000 shared-memory supercomputer. XAS data were measured at SSRL, which is supported by the Department of Energy, Office of Basic Energy Sciences Division. The SSRL Structural Molecular Biology Program is supported by the National Institutes of Health, National Center for Research Resources, Biomedical Technology Program, and by the Department of Energy, Office of Biological and Environmental Research.

Supporting Information Available: Cartesian atomic coordinates of the six-Cu model; MO energy levels with sulfur contributions for the tetrahedral sulfate dianion (Figure S1); atomic spin density plots for the three- and one-atom-bridged two-Cu models (Figure S2); energy level diagram showing mixing of virtual orbitals in radical monoanionic sulfate expressed using the MOs of C_s sulfate dianion (Figure S3); calculated distributions of sulfur 3p and 4p character in the unoccupied orbitals of [Cu(itao)SO_4], [Cu{$(CH_3)_6$tren}SO_4], and $ZnSO_4$ (Figure S4); sulfur K-edge spectra and second derivatives for [Cu(itao)SO_4] and [Cu{$(CH_3)_6$tren}SO_4], including fit and pseudo-Voigt lines (Figures S5 and S6, respectively); pseudo-Voigt components for fits to $CuSO_4$, [Cu(itao)SO_4], and [Cu{$(CH_3)_6$tren}SO_4] (Tables S1−S3). This material is available free of charge via the Internet at http://pubs.acs.org.

IC030311L